Initial localization and kinematic characteristics of the structural components of a coronal mass ejection

A. M. Uralov and V. V. Grechnev
Institute of Solar-Terrestrial Physics, Siberian Branch, Russian Academy of Sciences, Irkutsk, Russia

H. S. Hudson
Space Sciences Laboratory, University of California, Berkeley, California, USA

Received 2 December 2004; revised 4 February 2005; accepted 24 February 2005; published 27 May 2005.

[1] The leading component of a coronal mass ejection (CME), its observed frontal structure (FS), has been detected close to the solar surface in a few near-the-limb events only. Thus far, no manifestations of such a frontal structure have been reported in reasonable proximity to a preeruptive filament located away from the solar limb. Thus the identification of the FS with preevent coronal structures remains unclear. We propose a method to estimate the parameters of the initial volume of a CME, using comparative measurements of the spatial locations of the erupting filament and FS with a self-similar solution of the magnetohydrodynamic equations describing the expansion of the CME. We develop this method by analyzing observations of a large eruptive filament on the solar disk on 4 September 2000, using data acquired with the Solar Heliospheric Observatory (SOHO), Large-Angle Spectroscopic Coronagraph (LASCO), and EUV Imaging Telescope (EIT) instruments and the Siberian Solar Radio Telescope. We show that if a magnetic structure corresponding to the FS prior to the filament eruption does exist, then it is localized at a relatively low height (here, about 100–150 Mm above the filament). At the initial stage of the motion, the shape of the hot FS approximately reproduces the configuration of the cool eruptive filament. In addition, we conclude that the coronal dimming observed in this event could be also due to CME-caused suppression of the heating and/or mass supply of the dimmed structures rather than due to their opening only. We also obtain in a simple way an exact self-similar solution of MHD equations in a form suitable for analyses of experimental data.

Citation: Uralov, A. M., V. V. Grechnev, and H. S. Hudson (2005), Initial localization and kinematic characteristics of the structural components of a coronal mass ejection, *J. Geophys. Res.*, *110*, A05104, doi:10.1029/2004JA010951.

1. Introduction

[2] Many coronal mass ejections (CMEs), as observed by the Large-Angle Spectroscopic Coronagraph (LASCO) on SOHO, have the "three-part structure": a radially expanding cavity, a well-distinguished core, and a frontal structure (FS) which is the leading component of the visible CME. Also well-known is the similarity of such a CME's structure and that seen around a prominence on the solar limb if observed along the filament channel, which creates a coronal cavity between the prominence and the overlying coronal arcade [see, e.g., *Martin*, 1998; *Hudson et al.*, 1999]. One usually associates the core of the CME with an eruptive filament located either inside or adjacent to an active region prior to the eruption. The preevent location of the FS remains unknown, although observations of limb events clearly show that the FS forms above the preeruptive filament. In particular, the activation and slow ascent of the preeruptive filament is accompanied by the rise of one or more faint coronal loops visible only above the limb or in soft X rays [*Kano*, 1994]. After an acceleration typically at a rate of 0.5 km s^{-2} between 100 and 750 Mm above the solar surface, those loops probably form the leading edge of the CME [*Neupert*, 2002]. A first measurement of the kinematic characteristics of an ascending looplike CME's frontal structure was done by *Gallagher et al.* [2003]. They estimated the maximum acceleration of the FS to be about 1.5 km s^{-2} at a distance of 1.7 $R_\odot$ from the solar center.

[3] *Dere et al.* [1997] describe the first observation with SOHO/EIT (195 Å) and LASCO/C1-C2 (C1 is the innermost SOHO coronagraph; C2 observes the middle corona), where the propagation of the FS was reliably traceable from the CME initiation site up to several solar radii. In that case, the appearance of the CME was associated with the eruption of a small filament previously located on the solar disk near the limb. The authors conclude that the excitation of this CME occurred in a very small volume, with a size of about 35″. At the onset of the motion, the FS looks like an expanding circular loop (the interval between the EIT

0148-0227/05/2004JA010951$09.00

frames is about 12 min). One of the footpoints of this loop (its location on the disk is specified by the authors) is located, however, at a large distance from the visible center of the eruption, more than 100 Mm. It is not possible to find the initial position of the FS, but the mutual disposition of one of the FS bases and the ribbons of the associated two-ribbon flare implies that the magnetic loop corresponding to the FS was extended, before the eruption, along the same direction as the flare ribbons. Recently, *Cremades and Bothmer* [2004] have surveyed "structured CMEs," noting a strong tendency for self-similar development originating in compact loop structures. *Khan and Hudson* [2000] describe a different mechanism for FS formation in a particular class of CMEs, namely ones originating in trans-equatorial X-ray loops.

[4] The above facts characterize our present knowledge of the FS location at the initiation stage of a CME. It is difficult to understand the role of the FS in the existing theoretical schemes of the CME initiation. The magnetic field in the coronal cavity containing the filament likely has the same direction as the magnetic field along the axis of the filament inside it. The magnetic field direction in the coronal arcade is inclined or even perpendicular to the axis of the filament. Therefore a separatrix surface must exist to separate those magnetic domains. The existence of the FS itself hints at the presence of a separatrix surface between the coronal cavity (together with the filament inside it) and the overlying coronal magnetic arcade. It is not clear, however, which part of which domain best matches the frontal structure of the observed CME, nor where the FS mass originates. The FS is normally thought to have no importance in the CME initiation problem, but this is also not clear theoretically. Before being able to answer these questions, we must be able to identify the preevent volume whose magnetic structures subsequently form the FS. This volume seems to be closely related to that containing the initial energy of a CME.

[5] In this paper, by means of a particular example, we demonstrate a way to investigate the initial volume of a CME. The essence of this method is to use a self-similar solution of the MHD equations describing the expansion of a CME. *Zel'dovich and Raizer* [1966], *Sedov* [1981], *Barenblatt* [1978], etc., considered various examples of self-similar motions, their meaning, and the ways to obtain self-similar solutions of the gas-dynamics equations. *Low* [1982] first proposed describing solar coronal mass ejections in terms of self-similar solutions of the MHD equations. Appendix A contains a derivation of the basic expressions of self-similar motion that can be compared with an observed CME expansion. The solutions, similar to those found by *Low* [1982], are derived in a simple and clear way that facilitates their use in experimental data analyses. We compare the self-similar solutions with measures of kinematic quantities (velocity and height) of the CME components, the filament, and the FS. It then becomes possible to observe the motion of the CME core (erupting filament) during the whole acceleration stage of a CME and to estimate the size and geometry of the CME at the moment of its onset.

[6] The experimental data are based on the observations of a CME associated with the eruption of a quiescent filament on the solar disk, which occurred on 4 September 2000. The motion of the eruptive filament across the solar disk and up to almost two solar radii is measured from the observations with the Siberian Solar Radio Telescope (SSRT, 5.7 GHz [*Smolkov et al.*, 1986]; the current state of the SSRT was reported by *Grechnev et al.* [2003]). Beyond two solar radii, SOHO/LASCO/C2-C3 data are used. The propagation of the frontal structure ahead of the eruptive filament is analyzed using SOHO/EIT and LASCO images. We also analyze *Yohkoh*/SXT images observed before and after the eruption.

[7] The event of our interest was discussed previously in a paper by *Uralov et al.* [2002] (hereafter referred to as Paper 1), where we paid major attention to the CME initiation mechanism (dual-filament initiation model). Before the eruption, a large quiescent filament 1 (Figure 1c) was observed in Ha on the solar disk. A two-ribbon flare evolved after the eruption at the place of the preexisting filament. Its microwave emission was thermal throughout the flare. The eruption of the filament consisted of three stages. At the first stage, the filament ascended very slowly and did not show conspicuous helicity in its structure. At the second stage, the acceleration was maximal, and the filament took on a helical structure, but flare ribbons had not yet appeared. At the third stage, the filament already moved with a high velocity, but the acceleration was low. Flare ribbons appeared. Some SSRT images of this event are also shown by *Grechnev et al.* [2003].

[8] Because the conspicuous helical structure of the filament appeared before the flare itself, we connected its formation with the presence of the filament barbs. Their magnetic reconnection results in the formation of a helical magnetic field inside the eruptive filament which causes abrupt imbalance of the system: filament barbs/filament plus the magnetic field between the filament, and the overlying coronal arcades plus the overlying coronal arcades. In Paper 1 we supposed the existence of a coronal magnetic structure to consolidate the preeruptive filament segments interacting with each other. We assumed this structure to be localized in between of the filament and the overlaying coronal arcades and called it the backbone magnetic field. We also supposed the slow increase of magnetic flux to be the initial cause of the slow ascent of the preeruptive filament, the stretch of the filament barbs as well as their subsequent magnetic reconnection. The growth of the flux of this magnetic field is thus equivalent to the increase of the magnetic field flux within the coronal cavity embracing the preeruptive filament. We connected the presence of the backbone magnetic field with the formation of the CME's frontal structure, but it remains uncertain whether this is the case in reality or not.

[9] Our purpose is to estimate the initial size of a CME by a comparison of the analytic self-similar solution with measured height-time plots for both the eruptive filament and the FS. For the eruptive filament, we consider the height-time plot of the fastest part of its leading edge. This plot for the slow ascent and rapid acceleration stages measured from the SSRT images observed with an interval of 2 to 3 min is given in Paper 1. Here we supplement those data with measurements from SOHO/LASCO/C2-C3 to show the stage when the motion of the eruptive filament approaches nearly constant velocity. For the frontal structure, we use information from the SOHO/LASCO CME

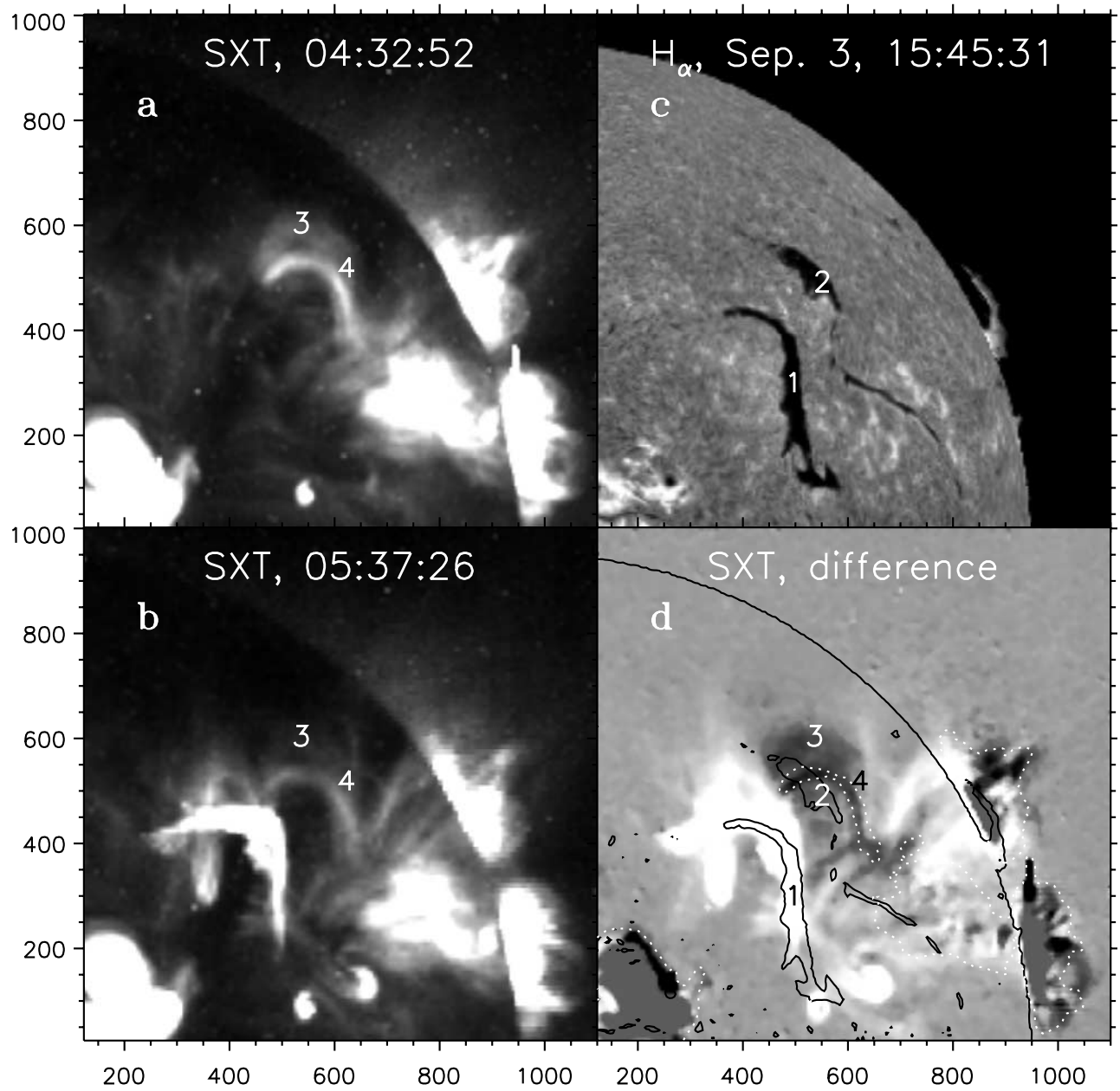

Figure 1. Soft X-ray and Hα images. (a) and (b) Preeruptive and posteruptive Yohkoh/SXT images (AlMg filter) and (d) their difference; (c) Hα filtergram, Big Bear Solar Observatory, 3 September 2000, 1546 UT (the previous day). Black contours in Figure 1d delineate filaments from the Hα image, and white dotted contours delineate bright loops in the preeruptive SXT image. Digits label filaments (1 and 2), broad dimming (3), loop structure (4).

catalog and involve additionally SOHO/EIT and *Yohkoh*/SXT images endeavoring to detect the FS as close to the filament as possible.

2. Observations

2.1. Soft X Rays and Hα

[10] Figures 1a and 1b show soft X-ray images observed with *Yohkoh*/SXT before and after the event, along with a preevent Hα image (Figure 1c). To coalign the images, we compensated for solar rotation as described by *Chertok et al.* [2004] and I. M. Chertok and V. V. Grechnev (Large-scale activity in the Bastille Day 2000 solar event, submitted to *Solar Physics*, 2005). Figure 1d shows a difference *Yohkoh*/SXT image obtained by the subtraction of the preeruption image of 0432:52 UT from the posteruption one, observed at 0537:26 UT, as a halftone background. Black contours on top of the image show filaments 1 and 2 present in the Hα filtergram (Figure 1c), and white dotted contours show a relatively bright loop observed in soft X rays. The event is associated with the eruption of filament 1, which disappears in Hα images after the event. The second filament 2 keeps its shape and position just after the eruption. It disappears later on, and Hα images do not

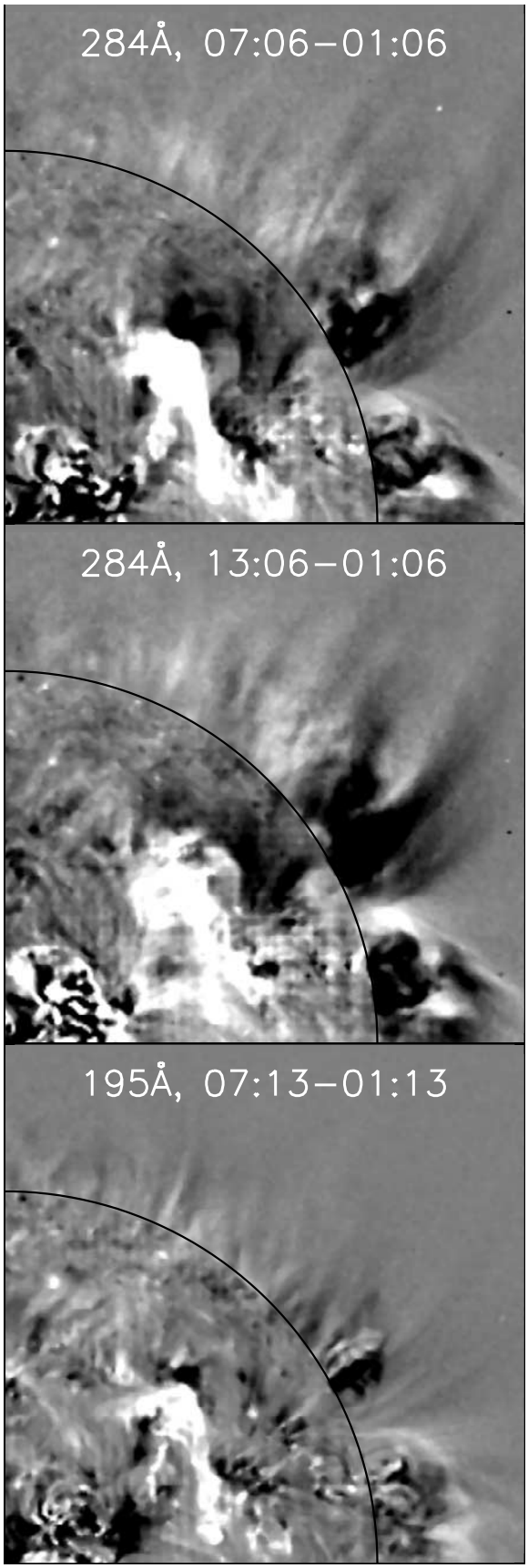

Figure 2. Base-difference SOHO/EIT images observed in two channels, (top and middle) 284 Å and (bottom) 195 Å. We show the NW quadrant only.

show it 10 hours after the eruption. The disappearance of filament 2 did not result from eruption; presumably, it either heated or otherwise dissolved.

[11] A broad dimming 3 appears after the eruption just northeast of the eruptive filament 1. This dimming includes a system of loops (visible in soft X rays) that does not disappear after the eruption but only decreases in brightness. The dimming embraces filament 2. The magnetic channel including filament 2 is nearly parallel to the channel of filament 1. The dimming is not uniform. Within dimming 3, a deeper narrow loop-like structure 4 (Figure 1d) starts and extends to the southwest. Its end passes into three or four dark loop-like structures. Other darkening regions visible in Figure 1d close to the solar disk center and on the limb are due to the saturation of the image of 0537:26 UT.

2.2. Extreme Ultraviolet

[12] Figure 2 shows difference images observed by SOHO/EIT in two channels, 284 Å and 195 Å. The high-temperature 284 Å channel shows essentially the same dimming structure as the *Yohkoh*/SXT images. This structure persists for several hours in 284 Å images, but it is not detectable in either of the lower-temperature channels. We show the 195 Å image as the highest temperature of the other EIT channels only.

[13] Running-difference EUV images shown in Figures 3a and 3b are produced from SOHO/EIT 195 Å heliograms (CME Watch Program, cadence 12 min). They display a faint emission feature (<0.5% of the maximum brightness of the frames) "S" similar to a coronal wave (sometimes referred to as an "EIT wave") running away from the eruption site. This structure ("S") is distinctly seen above the solar limb in Figure 3b (0536 UT). It can be detected still earlier, at 0524 UT (bright structure "S" in Figure 3a), when the eruptive filament ("F," black in Figures 3a and 3b) only starts to acquire its velocity. It is observed well ahead of the filament ("F") and runs considerably faster than the eruptive filament, as the comparison of Figures 3a and 3b shows. This faint feature expands in the same way as the CME's frontal structure; as the time-height plots in Figures 5a and 5b further show, it coincides with the FS kinematically and increasingly takes its shape. For these reasons we identify this feature with the CME's frontal structure. In this case, the FS is detectable even on the solar disk, and we were lucky to detect it.

[14] The fact that the frontal structure is detectable in SOHO/EIT 195 Å images means that at least some part of it has a temperature of order 1.5 MK at a distance of order of a solar radius from the eruption site, which is in accord with the observations reported by *Dere et al.* [1997]. At the same time, the absence of the southern FS component in Figure 3a is noteworthy. On the contrary it dominates the northern FS component in Figure 3b. Plasma cooling in the FS expansion can explain this. If the temperature of the southern FS component significantly exceeds 1.5 MK at 0524 UT, then its appearance at 0536 UT can be associated with its cooling up to a temperature of order 1.5 MK. In turn, the cooling of the northern S component results in the temperature decrease of some part of its material well below 1.5 MK at 0536 UT and, consequently, to the decrease of the emission in 195 Å line.

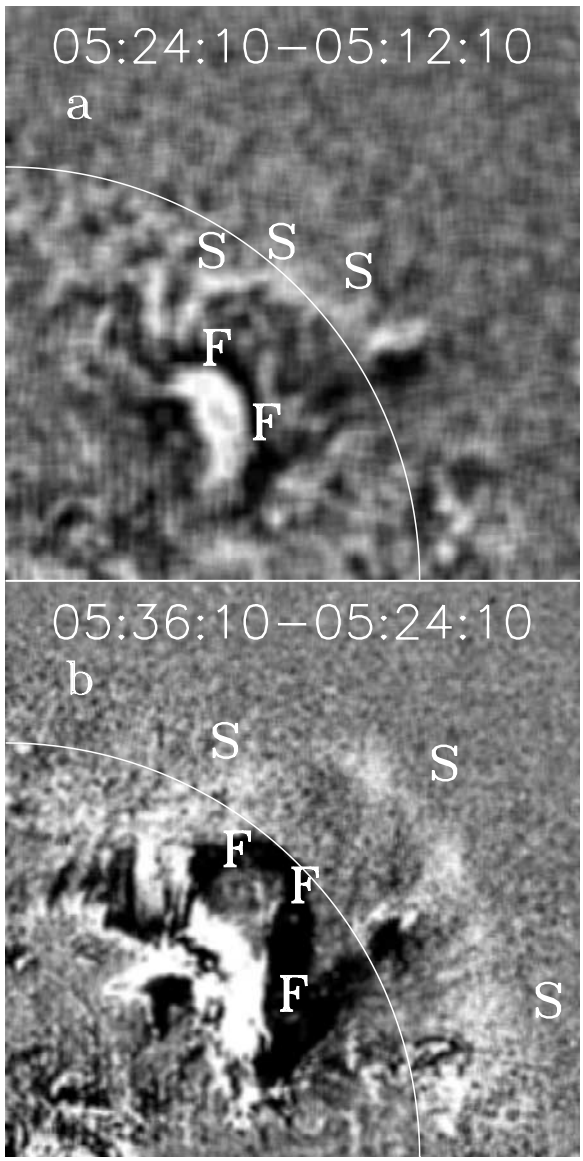

Figure 3. Running-difference SOHO/EIT 195 Å images demonstrating the propagation of the CME frontal structure ("S"): (a) on the disk, 0524 UT; (b) above the limb, 0536 UT. The eruptive filament is labeled "F." We show the NW quadrant only. The brightness range is ±3 (Figure 2a) and ±5 (Figure 2b) EIT counts. The images are smoothed with a width of 3 (Figure 2a) and 7 (Figure 2b).

2.3. SOHO/LASCO Images

[15] The difference images in Figure 4 show the appearance of the CME's structural components within the field of view of the LASCO/C2 coronagraph ($R > 2R_{\odot}$) from behind the occulting disk. First, the frontal structure "S" appears at 0606 UT (Figure 4a), then the eruptive filament "F" becomes visible at 0654 UT (Figure 4b). A great deal of similarity of these structures is conspicuous. Their shapes resemble the structure visible in EIT image (Figure 3b) also. One can now see from the LASCO observations that each of the structures consists of two components, the northeast and southwest ones. In Figure 3a and 3b, only the southwest FS segment is present, clearly visible in EUV. The corresponding segment of the eruptive filament is also more pronounced in the Hα and EUV images. At the same time, the twin-filament structure of the expanding eruptive filament is detectable in the microwave emission (SSRT, 5.7 GHz) where the propagation of both segments around the solar limb was observed. These observational facts were discussed in Paper 1 in the context of the dual-filament initiation model of a CME.

[16] We also note the displacement of the coronal ray northward caused by the ejection that shows up in the difference image as a brightening of the northern edge of the ray with the darkening of its central part. The displacement is more pronounced in later SOHO/LASCO images.

2.4. Height-Time Plots

[17] Figure 5a shows height-time plots of the eruptive filament and the frontal structure of the CME. The distance

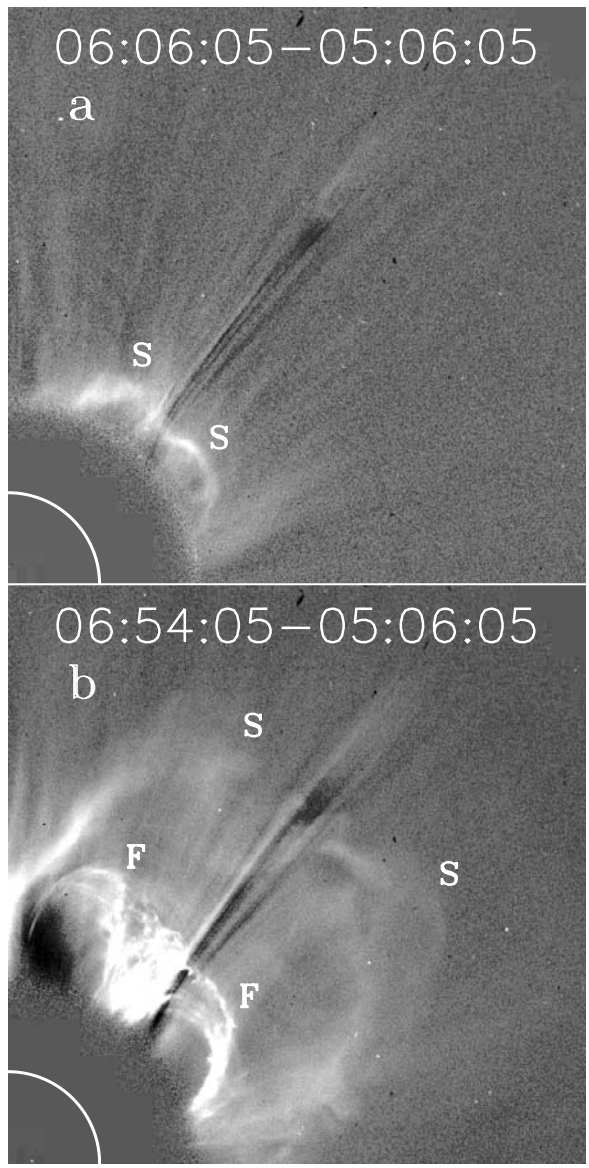

Figure 4. Base-difference SOHO/LASCO/C2 white light images showing the appearance from the occulting disk ($R > 2R_{\odot}$); first, (a) the frontal structure "S" and next, (b) the eruptive filament "F." We show the NW quadrant only.

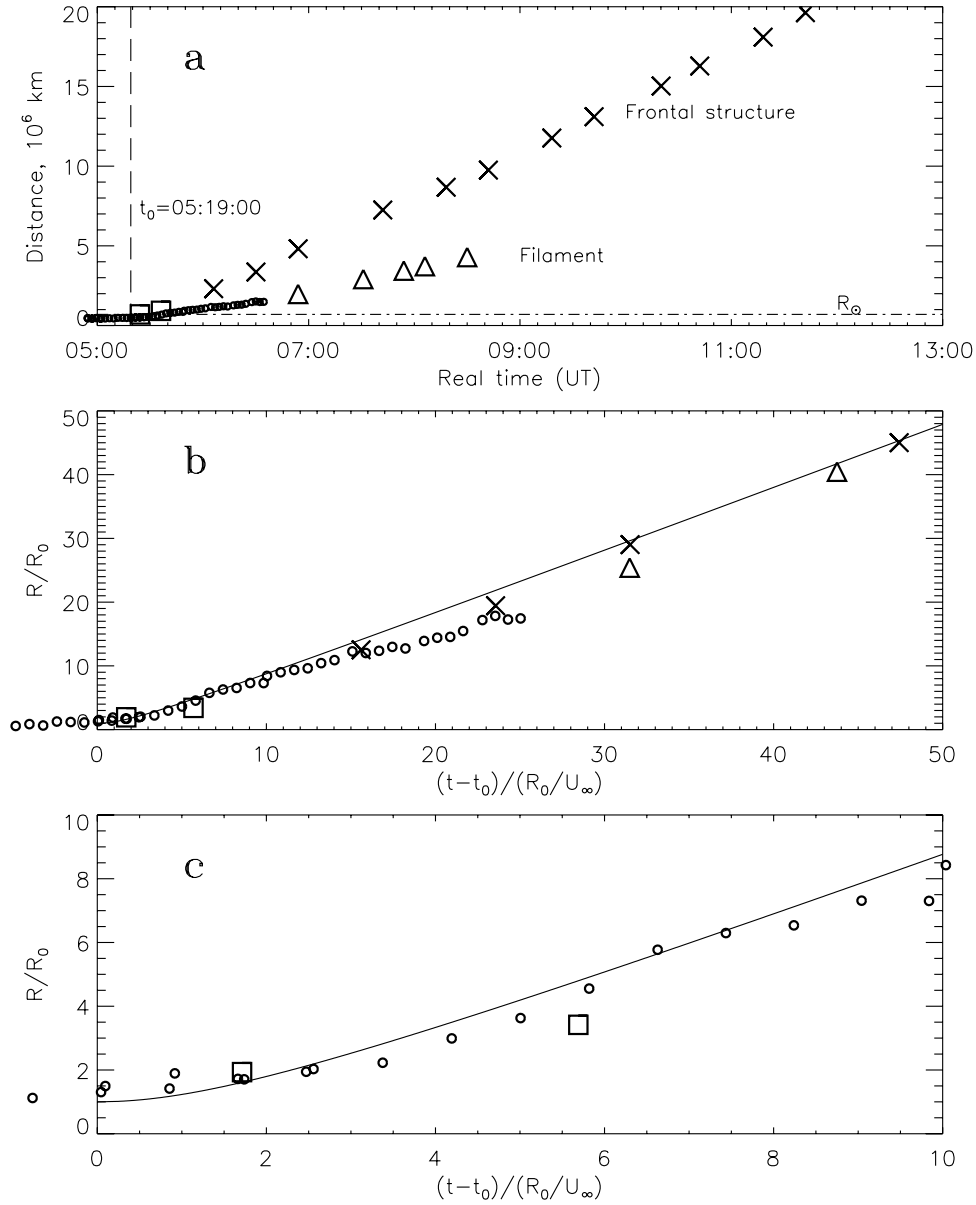

Figure 5. Height-time plots of the eruptive filament and the frontal structure of the CME. (a) Experimental data. The positions of the filament are marked with small circles (SSRT) and triangles (LASCO), and those of the frontal structure are marked with squares (EIT) and crosses (LASCO). The horizontal axis shows universal time, and the vertical axis shows the distance from solar disk center. (b) A comparison of the experimental height-time plots with the self-similar invariant kinematic plots. The horizontal axis shows the dimensionless time $(t - t_0)/\tau$, with τ being the initial CME timescale. The vertical axis shows the dimensionless coordinate $x = R_s/R_{0,s}$, with R_s being the distance measured from the virtual expansion center and $R_{0,s}$ being the initial radius of the CME. (c) Same as Figure 5b, the initial part.

is measured from the solar disk center approximately along the same radial direction with a position angle ≈315°. Along this direction, the apparent expansion of the CME is close to the radial practically from the onset of its motion. The measured heights of the filament are marked with small circles (SSRT) and triangles (LASCO). The heights of the FS are marked with crosses (LASCO) and squares (EIT). The similarity of the plots and shapes of the FS and the filament (see Figure 4b) provides a basis for the self-similarity approach to the expansion of a CME [*Low*, 1982] and for its usage to estimate initial parameters of the CME.

3. Discussion

3.1. Dimming

[18] The *Yohkoh*/SXT images available do not show anything directly associated with the FS of the preeruptive filament of interest (1 in Figure 1). There is, however, an interesting feature probably related to the magnetic structure

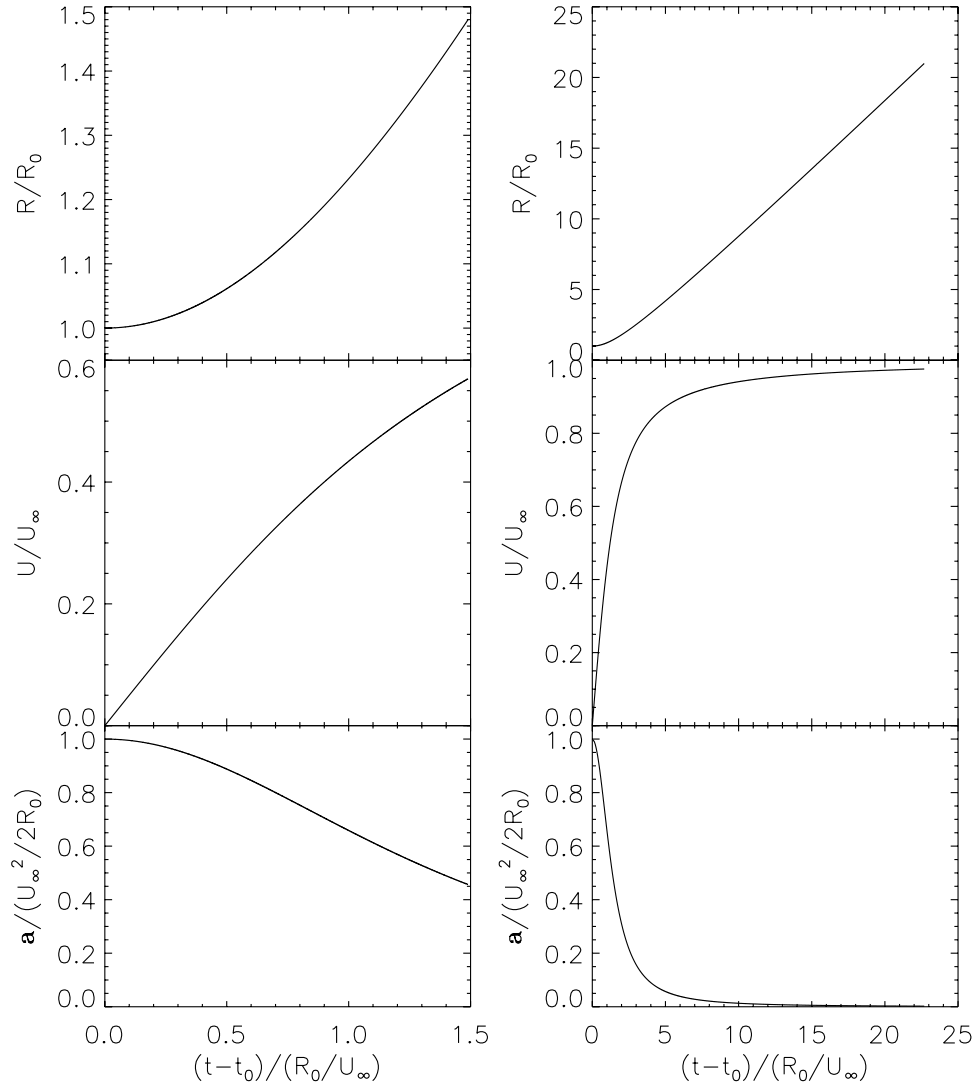

Figure 6. Invariant kinematic plots to describe a self-similar expansion. (left) Extended initial part; (right) wider range.

enveloping quiescent filaments. There is a loop system 3 and 4 observed in soft X rays in the dimming region. That is, the dimming is due to the darkening of the whole arcade consisting of several magnetic loops. As we noted in section 1, the existence of an arcade above a coronal cavity containing the filament necessarily implies the presence of a separatrix surface between their magnetic fields. The presence of this separatrix surface suggests the heating and mass supply to the coronal arcade observed [see, e.g., *Wang et al.*, 2000]. The dimming observed above filament 2 (Figure 1) is likely related to such a current-carrying surface.

[19] Loop 4 together with the loop system at its southwest end does not disappear after the eruption, but only decreases its brightness. The features keep their shapes and positions. We cannot follow the evolution of these loops between 0432:52 and 0537:26 UT because of the lack of *Yohkoh*/SXT data in this interval. We can only state definitely that loop 4 does not become darker before the eruption, but still brighter, in the interval 0355:34–0432:52 UT. The same is true for the broad dimming 3 also.

[20] Dimmings are generally interpreted as density depletions in the course of the opening of a magnetic loops into the solar wind. However, the opening and subsequent restoration of a loop at the same place and with the same shape seems physically improbable, but homologous dimmings have been observed [see *Chertok et al.*, 2004]. In our case, it is not possible to determine the nature of the dimmings because of limited *Yohkoh*/SXT data in the interval of interest. Therefore we can state only that in this case either the mass supply to the loops or their heating becomes partially suppressed or the darkening of all the loops is not related to the eruption, which looks unlikely. We note herewith that EIT images in all but 284 Å channels do not show the broad dimming visible in soft X rays but footpoint regions only (see Figure 2). The fact that the darkened loop system remains invisible in lower-temperature EIT channels suggests that the dimming is not due solely to a temperature decrease. Alternatively, one could have a temporary suppression of the mechanism responsible for the mass supply to the arcade loops or a joint variation of temperature and density that could produce such an

effect. This disturbance is definitely connected with the eruption that occurred nearby and possibly reflects the fact of the perturbation of all magnetic structures adjacent to the initial volume of the CME, as in the cases studied by *Chertok et al.* [2004]. This phenomenon seems to be interesting enough to be studied elsewhere in the context of dimming mechanisms also. Note that a similar phenomenon was presented (but not discussed) by *Harrison et al.* [2003] in their Figure 5, where the corona gradually darkens, but the dimmed loops remain closed.

3.2. Kinematic Characteristics

[21] To understand how to compare the plots shown in Figure 5a with the analytic description of a self-similar expansion (Figure 6), we give the necessary expressions as derived in Appendix A. Let the initial expanding velocity of the CME be zero, $U_0 = 0$, neglecting the very small preeruptive velocity of the filament. Next, from the solutions (A4), (A9), and (A10) given in Appendix A, we obtain the following expressions:

$$\eta = \frac{U_{\infty,p}}{U_{\infty,s}} = \frac{U_p(t)}{U_s(t)} = \frac{R_{0,p}}{R_{0,s}} = \frac{R_p(t)}{R_s(t)}, \tag{1}$$

$$\frac{t - t_0}{\tau} = \sqrt{x}\sqrt{x-1} + \ln\left(\sqrt{x} + \sqrt{x-1}\right), \tag{2}$$

$$\tau = \frac{R_{0,s}}{U_{\infty,s}} = \frac{R_{0,p}}{\eta U_{\infty,s}},\ x = \frac{R_s}{R_{0,s}} = \frac{R_p}{R_{0,p}},$$

$$U_s = \frac{dR_s(t)}{dt} = \frac{1}{\eta}U_p = U_{\infty,s}\sqrt{1 - \frac{R_{0,p}}{R_p}},\ U_p = \frac{dR_p(t)}{dt}, \tag{3}$$

$$a_s = \frac{dU_s(t)}{dt} = \frac{1}{\eta}a_p = \frac{\eta U_{\infty,s}^2}{2}\frac{R_{0,p}}{R_p^2},\ a_p = \frac{dU_p(t)}{dt}. \tag{4}$$

Here R_p and R_s are the distances of the eruptive filament (subscript "p" denotes the prominence, and "s" denotes frontal structure) and the frontal structure from some expansion center whose position is determined later. $R_{0,p}$ and $R_{0,s}$ are the initial values of these quantities corresponding to $t = t_0$, and U_p and U_s are the velocities of the filament and the FS. Here a_p and a_s are the accelerations. $U_{\infty,p}$ and $U_{\infty,s}$ are the asymptotic values of the U_p and U_s, reachable when $t \to \infty$. We can take them equal to the values of $U_p(t)$ and $U_s(t)$ measured far from the solar surface, when the velocities of the FS and the eruptive filament (the core of the CME) are nearly constant (see the height-time plots in Figure 5a). The ratio of these velocities is constant if the expansion is self-similar: $\eta = U_p(t)/U_s(t) = const$. In our case, $U_{\infty,p} \approx 360$ km/s and $U_{\infty,s} \approx 900$ km/s, so $\eta = 0.4$. The expansion center is not known a priori, so we express the distances $R_p(t)$ and $R_s(t)$ in terms of a distance r' measured from the initial position of the corresponding piece of the filament before the eruption:

$$R_p(t) = R_{0,p} + r'_p, \qquad R_s(t) = R_{0,p} + r'_s. \tag{5}$$

[22] The virtual expansion center is located at a distance of $R_{0,p} = R_p(t = t_0)$ from the initial position of the filament toward the solar disk center. In principle, the distance $R_{0,p}$ can be found directly from the experimental dependence $U_p(r'_p)$ under the assumption of the self-similarity of the expansion. For this purpose, one should measure exactly the value of $U_p(r'_p)$ at least at one point r'_p, and use the expressions (3) and (5). However, we have not yet justified the self-similarity assumption for our example, nor does the measurement accuracy allow to us evaluate $U_p(r'_p)$ reliably at the CME acceleration stage. These circumstances force us to use another technique.

[23] We want to compare the solution (2) with the height-time plots of Figure 5a where a new variable (5) is used instead of the distance from the solar disk center. If we put a value of t_0 into expression (2) and vary $R_{0,p}$, then it is possible to find a value of the latter quantity bringing the calculated curve into satisfactory accord with the experimental data set. Then, using the value of $R_{0,p}$ found, we are able to calculate $R_{0,s}$, characterizing the initial size of the CME, from expression (1). One should be aware that the self-similar solution could not describe the expansion process of a CME entirely, and we can only use it to estimate the characteristic spatial scale of the problem. We thus take the initial value of this parameter as an estimate of the initial size of the CME. In addition, the measurement accuracy for the position of the filament at the fast acceleration stage determines the uncertainty of the $R_{0,p}$ thus obtained. Similar circumstances govern the estimation of the onset time t_0. One should keep in mind here that the filament moves with a small constant velocity even before t_0.

[24] According to (4), the onset of the self-similar expansion corresponds to the highest acceleration of the filament, $a_{\max,p} = (U_{\infty,s}^2/2) \times (\eta^2/R_{0,p})$. However, it is difficult to catch the onset time precisely, because the velocity of the filament U_p and its displacement $\Delta r'_p$ within the sampling interval are small at that time, and the measurement accuracy is not sufficient. Expressions (2), (3), and (5) as well as Figure 6 show that at the early initial stage of the expansion close to t_0, $r'_p(\ll R_{0,p}) \propto (t - t_0)^2$, $U_p(r'_p \ll R_{0,p}) \propto (t - t_0)$ so that the self-similar expansion mimics a uniformly accelerated motion. Then, with the increase of the distance $r'_p(t)$, its time dependence approaches the linear one.

[25] The initial time t_0 corresponds to the onset of the nonlinear part in the $r'_p(t)$ dependence. This is detectable in the experimental height-time plot and is approximately 0520 UT. This value of t_0 can be taken as a first approximation in the fit of the expected, calculated relation to the experimental data set. Next, trying to bring the asymptotic nearly linear long-distance parts of the expected and calculated height-time plots into the approximate coincidence, we fit the $R_{0,p}$ value. Then we repeat the fitting process iteratively, thus alternately improving the approximations of t_0 and $R_{0,p}$.

[26] The result of the fitting is shown in Figures 5b and 5c. The horizontal axis shows the dimensionless time $(t - t_0)/\tau$

with the initial CME's timescale being $\tau = R_{0,s}/U_{\infty,s} = R_{0,p}/U_{\infty,p}$; see (2). The vertical axis shows the dimensionless coordinate $x = R_s/R_{0,s} = R_p/R_{0,p}$ with R_p and R_s defined by the expressions (5). When these invariant dimensionless coordinates are used, both experimental height-time plots shown in Figure 5a are converted into a single plot. The correspondence of this plot with the self-similar solution (2) is satisfactory but not perfect. The parameters of the self-similar expansion shown by the solid line are as follows:

$$\begin{aligned} &U_{\infty,p} \approx 360 \text{ km/s}, \; U_{\infty,s} \approx 900 \text{ km/s}, \quad \eta = 0.4 \\ &t_0 = 05:19 \text{ UT}, \quad \tau \approx 170 \text{ s}, \\ &R_{0,p} \approx 60 \text{ Mm}, \quad R_{0,s} \approx 150 \text{ Mm}, \\ &R_{0,s} - R_{0,p} \approx 90 \text{ Mm}, \\ &a_{\max,p} \approx 1.1 \text{ km/s}^2, a_{\max,s} \approx 2.7 \text{ km/s}^2. \end{aligned} \tag{6}$$

The values of $R_{0,p}$, $R_{0,s}$, $a_{\max,p}$, and $a_{\max,s}$ obtained are of course approximations. The difference $R_{0,s} - R_{0,p}$ is an estimate of the distance between the apparent position of the filament and the inferred position of the FS just before the eruption.

[27] Since the eruptive phenomenon discussed occurred on the solar disk rather than of the limb, we should take into account the aspect angle assuming the motion of the eruptive filament normal to the solar surface. In this case, all the parameters (6) containing the length dimension should be multiplied by $1/\sin\varphi \approx 1.4$, where $\varphi \approx 45°$ is the angular distance from the solar disk center. The values τ and η remain unchanged. After such a correction, the height difference of the preeruptive FS and filament is $\Delta h_0 = R_{0,s} - R_{0,p} \approx 125$ Mm, the initial acceleration FS is $a_{\max,s} \approx 3.8$ km/s^2, and $R_{0,p} \approx 85$ Mm, $R_{0,s} \approx 210$ Mm, $U_{\infty,p} \approx 500$ km/s, $U_{\infty,s} \approx 1260$ km/s. Note that our estimate of the maximum acceleration is of the same order as that one measured by *Gallagher et al.* [2003] for a quite different event.

[28] Now we should take into account the height of the eruptive filament itself. One hour before the eruption, its upper edge was as high as about 70 Mm, which can be found from SOHO/EIT images and the initial position of the filament on the disk. The lower edge of the filament was close to the solar surface, as established by the daily Big Bear Hα observations of this quiescent, long-lived filament during its appearance at the east limb. The microwave and EUV images of this filament resemble each other (Paper 1). On the basis of this fact, we measured the position of the filament in SSRT microwave images approximately from its centroid; hence the initial height of the filament is $h_{0,p} \approx 35$ Mm in our measurements. Therefore the virtual expansion center of the CME is located below the solar surface at a depth of $h_{0,p} - R_{0,p} \approx -50$ Mm, and the preeruption height of the FS above the solar surface is $h_{0,s} = (R_{0,s} - R_{0,p}) + h_{0,p} \approx 160$ Mm.

[29] Let us estimate now the volume of the solar atmosphere involved in the CME structure. This is the region determined by the intersection of the solar surface (we assume it flat for simplicity) with a sphere of radius $R_{0,s} \approx 210$ Mm around the virtual expansion center. The height of the segment is also known, $h_{0,s} \approx 160$ Mm. The radius of the segment base is $L = \sqrt{h_{0,s}(2R_{0,s} - h_{0,s})} \approx 204$ Mm, and its volume is $W = \pi h_{0,s}^2(3R_{0,s} - h_{0,s}) \approx 3.8 \times 10^{31}$ cm^3. A circle with diameter $2L \approx 400$ Mm delimits a part of the solar surface that can be called the "domain of influence," which determines the appearance and development of the CME. Note that the distance between the farthest points of the flare ribbons observed in EUV for the entire event is also about 400 Mm. This could be a coincidence, considering our very approximate estimates. Nevertheless, it seems reasonable that the domain of influence should be comparable in size with the scale of the flare ribbons.

[30] If we assume an average plasma number density of $\langle n \rangle = 10^8$ cm^{-3} inside the initial CME's volume of $W \approx 3.8 \times 10^{31}$ cm^3, we estimate its mass to be $m \approx 6.5 \times 10^{15}$ g. Alternatively, an assumed density of $\langle n \rangle = 10^9$ cm^{-3} over the area of the domain of influence, with the hydrostatic law for the corona, gives a comparable mass. This is sufficient for a major CME even without the additional mass of the filament itself.

[31] To estimate the total energy of the CME, we make use of its self-similar expansion. This implies that the stored energy within the initial volume of the CME is completely spent to accelerate the CME and to overcome the force of gravity. In the asymptotic limit, the entire energy is concentrated in the kinetic energy, whose minimum value in our event is $m\langle v_\infty^2 \rangle/2 \approx m\langle U_{\infty,p}^2 \rangle/2 \approx 8 \times 10^{30}$ erg. Here, $\sqrt{\langle v_\infty^2 \rangle}$ is the average mass velocity which we assumed to be equal to the mass velocity of the eruptive filament $U_{\infty,p} \approx 500$ km/s so that the entire CME mass would be concentrated in the filament. Next, we can use the estimate of the average mass velocity of the CME according to (A13):

$$\langle v_\infty^2 \rangle \approx \left[\frac{2C_0^2}{\gamma(\gamma - 1)} + V_{a0}^2 - V_{\text{esc}}^2 \right], \tag{7}$$

with $V_{\text{esc}} \approx 618$ km/s the escape velocity at the solar surface, γ is the polytropic index, and C_0^2 and V_{a0}^2 are the average squared sound and Alfvén velocities in the initial volume of the CME. The fact that the right-hand side of expression (7) is positive means that a self-similar solution corresponding to the unlimited expansion of the CME does exist. Either an increase of the magnetic field or temperature or a decrease of the average density inside the initial CME volume favors this. With $\gamma = 4/3$, which is the existence condition of the accurate self-similar solution, and the initial plasma temperature of the CME of $T_0 = 2$ MK, according to (7), the value of $\langle v_\infty^2 \rangle \approx U_{\infty,p}^2 = (500 \text{ km/s})^2$ implies a velocity $V_{a0} \approx 660$ km/s. This Alfvén velocity corresponds to the minimum value of the average magnetic field inside the initial CME volume of $B_{\min} = 3$ G with the minimal average number density of $\langle n \rangle = 10^8$ cm^{-3}. These values of γ, T_0, $B_{\min}$ and W lead to an initial total magnetic and thermal plasma energy content of $(B_{\min}^2/8\pi)W + 2nkT_0W/(\gamma - 1) = 2 \times 10^{31}$ erg, which is 2.5 times greater of 8×10^{30} erg, the entire kinetic energy of the CME at the end of the expansion. The

difference of these energies is spent to overcome gravity.

[32] Concluding this section, let us return to the last paragraph of section 2.2 where we connected the appearance of the FS in the EUV images with plasma cooling in the expanding CME's frontal structure. The self-similar expansion of the CME is accompanied by an adiabatic temperature decrease of its components (see also (A1) and (A2)) so that the FS plasma temperature is $T_s = T_{0,s}(R_{0,s}/R_s)^{3/(\gamma-1)}$. With the values $R_{0,s}$ and R_s already known corresponding to the EUV FS images in Figure 3, we can estimate the expected variation of T_s. The ratio $R_s/R_{0,s}$ is equal to the ratio R/R_0 plotted in Figure 5b and 5c (EUV images are shown by squares). With $\gamma = 4/3$, the temperature of the FS decreases approximately by a factor of 1.8 between Figures 3a and 3b. Assuming the temperature of the brightest parts of the frontal structure, northern in Figure 3a and southern in Figure 3b, to be 1.4 MK, we estimate an initial temperature of $T_{0,s} \approx 2.7$ MK for the northern part of the FS and $T_{0,s} \approx 4.8$ MK for its southern part. The faintness of the frontal structure along with its temperatures, which we estimated for this event, show why it is very difficult to observe it before the eruption.

4. Summary

[33] We have discussed an example in which the source of a CME was an eruption of a large quiescent filament located beyond an active region and surrounded by weak, large-scale magnetic fields. Using this event as an example, we develop a technique for comparing the measured height-time plots of different structural components of the CME with a self-similar description. Such a comparison allows us to estimate the extent of the initial CME volume, both surface ($2L$) and height ($h_{0,s}$). The surface scale of the solution characterizes the solar-surface area that participates in the formation and subsequent evolution of the CME. In particular, the surface size of the CME appears comparable with the maximum extent of the flare ribbons. The initial acceleration of the CME is of order of some km/s^2. We estimate the initial height of the CME frontal structure $h_{0,s} \approx 160$ Mm which corresponds to its initial location at a height of $\Delta h_0 \approx 125$ Mm above the preeruptive filament. Such scales are comparable with the coronal cavities surrounding quiescent filaments (e.g., *Hudson et al.* [1999]). One can therefore assume that the frontal structure in the event considered is localized above the filament near the separatrix surface confining the coronal cavity. We have discussed a possible observable manifestation of the separatrix surface in soft X rays. A faint hot loop system was observed in that case at a height of about 100 Mm above the filament visible in Hα.

[34] Despite the closeness of the heights of the frontal structure and the coronal cavity, the former hardly is a simple copy of the upper part of the moving separatrix surface that confines the cavity. At the initial stage of the CME expansion, the main part of the frontal structure is possibly a large-scale loop structure extended along the eruptive filament and resembling its leading edge. At least, some part of the material of the frontal structure has a temperature of order 1.5 MK at a distance of order of one solar radius from the eruption site. Its initial temperature can significantly exceed this value.

Appendix A: Self-Similar Expansion of a CME

[35] As we mentioned in section 1, *Low* [1982] first proposed describing CMEs in terms of self-similar solutions of the MHD equations. However, the formal solution he obtained (equation (34) in the work of *Low* [1982]) is not convenient for experimental data analyses. This appendix shows how to obtain it in a form more suitable to analyze experimental data we have. Moreover, here we derive an exact self-similar solution in a simpler, demonstrative way, which we believe will be clear for readers.

[36] Let us consider an expanding volume of magnetized plasma. The shape of the surface $\Omega = \Omega(t)$ confining the expanding volume can differ from a sphere. The task is solved under additional assumptions. Namely, the radial velocity field $v = v_r(r, \theta, \varphi)\mathbf{e_r}$ is specified with the radius r measured from some center of the symmetry "O." Each packet of plasma moves in a straight line but expands as would an element interior to a ball expanding from the center "O." We also assume that the spatial distribution of each of the physical parameters $\Pi = \{\rho, p, v_r, B_r, B_\theta, B_\varphi\}$ inside the expanding volume always remains self-similar, $\Pi = \Pi_1(\Re)\tilde{\Pi}(\xi, \theta, \varphi)$. Here $\xi = r/\Re$ is the self-similar variable and $\Re = \Re(t)$ is some spatial scale characterizing the size of the expanding region at the instant t. The parameters ρ, p, B_r, B_θ and B_φ are the number density, plasma pressure, and the magnetic field components. It is convenient to choose the $\Re$ to be equal to the maximum distance from the surface Ω to the symmetry center "O." In such a case the parameters $\Pi_1 = \{\rho_1, p_1, v_{r1}, B_{r1}, B_{\theta 1}, B_{\varphi 1}\}$, varying in time, correspond to their values at points on the surface Ω, where $\xi = 1$. If the surface is a sphere, then the condition $\xi = 1$ is true at the whole surface Ω, and the values Π_1 determine some characteristic values of the physical parameters. The dimensionless functions $\tilde{\Pi} = \{\tilde{\rho}, \tilde{p}, \tilde{v}_r, \tilde{B}_r, \tilde{B}_\theta, \tilde{B}_\varphi\}$ do not depend explicitly on time. The functions $\Re(t)$, $\Pi_1(\Re)$, and $\tilde{\Pi}(\xi, \theta, \varphi)$ are found from the ideal MHD equations if the solution Π does indeed exist.

[37] Expressions for $\Pi_1(\Re)$ can be easily obtained under the conservation of the total mass m of material confined by the surface Ω. This condition is not valid if Ω is, for example, a shockwave front. In that case, the total mass involved in the motion continuously increases (however, if behind the shock front a contact discontinuity exists through which mass transfer does not occur, the mass will be conserved inside the volume confined by the discontinuity). The condition $m = const$ corresponds to an expansion of a gas ball into vacuum or into a medium of negligibly small density and pressure. With a dependence chosen, $\rho = \rho_1(\Re)\tilde{\rho}(\xi, \theta, \varphi)$, the mass of gas is $m = \rho_1(\Re)\Re^3 const_\rho$ with $const_\rho = \int \tilde{\rho}(\xi, \theta, \varphi)\xi^2 \sin\theta d\theta d\varphi d\xi$. The equality $m = const$ leads to: $\rho_1(\Re) = \rho_0(\Re_0/\Re)^3$ so that

$$\rho = \rho_0(\Re_0/\Re)^3\tilde{\rho}(\xi, \theta, \varphi), \tag{A1}$$

where $\rho_0 = \rho_1(\Re_0)$ is a characteristic plasma density at the initial moment $t = t_0$, and $\Re_0$ is the initial value of $\Re$. The variation of the gas pressure follows from the entropy equation, $d(c_v \ln(p/\rho^\gamma))/dt = 0$ with γ being the polytropic

index. The quantity $d/dt = \partial/\partial t + (\mathbf{v}\nabla)$ is the Lagrangian derivative characterizing the variation of some quantity within an individual packet of a moving medium whose mass is conserved. With a constant heat capacity c_v inside such an element, $p/\rho^{\gamma} = const$; then, taking (A1) into account, we obtain

$$p = p_0(\Re_0/\Re)^{3\gamma}\widetilde{p}(\xi, \theta, \varphi), \tag{A2}$$

where $p_0 = p_1(\Re_0)$ is a characteristic gas pressure at $t = t_0$.

[38] The components of the magnetic field B_r, B_θ, and B_φ inside the individual plasma packet can be found from the frozen-field condition. Let us select three orthogonal cross sections within the packet, $dS_\varphi = rdrd\theta = \Re^2\xi d\xi d\theta$, $dS_\theta = r\sin\theta d\varphi dr = \Re^2\xi\sin\theta d\varphi d\xi$, and $dS_r = r^2\sin\theta d\varphi d\theta = \Re^2\xi^2\sin\theta d\varphi d\theta$. $\theta d\varphi d\theta$. The conservation of the magnetic fluxes $B_\varphi dS_\varphi$, $B_\theta dS_\theta$, and $B_r dS_r$ in the spherical expansion of the packet (with ξ,θ, φ, $d\xi$, $d\theta$, and $d\varphi$ being invariable) means that all the three magnetic field components change synchronously:

$$\{B_r, B_\theta, B_\varphi\} = \{B_{r0}, B_{\theta 0}, B_{\varphi 0}\}(\Re_0/\Re)^2\left\{\widetilde{B}_r, \widetilde{B}_\theta, \widetilde{B}_\varphi\right\}. \tag{A3}$$

Here $\{B_{r0}, B_{\theta 0}, B_{\varphi 0}\}$ are the characteristic values of the magnetic field components at the initial instant of time, when $\Re = \Re_0$. Note that synchronous time variation of all the three components does not take place in a flat or cylindrical geometry.

[39] The spatial profiles (A1), (A2), and (A3) stretch radially, being proportional to $\Re(t)$. Thus each point of the self-similar profile $\xi = const$ moves along the characteristic line $dr/dt = \xi d\Re/dt = V_r$. This expression follows directly from the equality $d\xi/dt = d(r/\Re)/dt = 0$. In a general case of self-similar motions, the velocity V_r does not coincide with the actual mass velocity $v_r = v_{r1}\widetilde{v}_r(\xi, \theta, \varphi)$, but in our particular case this is true. Taking $v_{r1} = d\Re/dt$ and substituting (A1) into the continuity equation expressed in the form

$$d\rho/dt = -\rho(\partial v_r/\partial r) - (2\rho v_r)/r,$$

we obtain

$$3 = (\partial\widetilde{v}_r/\partial\xi) + 2\widetilde{v}_r/\xi.$$

The solution of the last equation is a function $\widetilde{v}_r = \xi$, therefore

$$V_r = v_r = \xi d\Re/dt. \tag{A4}$$

In the derivation of expression (A4) from the continuity equation, it is sufficient to use the explicit time differentiation of expression (A1). This simplification applies for the given task only, with $m = const$, and with all the same pieces of mass being involved into the self-similar motion. In the general case, however, one should use directly the form $\partial/\partial t + (\mathbf{v}\nabla)$ of the substantial derivative d/dt.

[40] So far we have simply assumed that a self-similar solution of the problem does exist. Now let us make sure that it is the case and find the $\Re(t)$ dependence. We will use the momentum equation in the form

$$\rho\frac{d\mathbf{v}}{dt} = \frac{1}{4\pi}\mathbf{rotB}\times\mathbf{B} - \mathbf{grad}p - \rho\frac{GM_g}{r^2}\mathbf{e_r} = \mathbf{F}_B + \mathbf{F}_p + \mathbf{F}_g, \tag{A5}$$

with a central gravity force due to some mass M_g introduced for generality and G being the gravitational constant. By substituting (A1)–(A4) into the expressions for forces and taking into account that $\partial/\partial r = (1/\Re)\partial/\partial\xi$, we obtain

$$\mathbf{F}_B = B_0^2\left(\frac{\Re_0}{\Re}\right)^4\frac{\mathbf{f}_B(\xi,\theta,\varphi)}{\Re}, \quad \mathbf{F}_p = -p_0\left(\frac{\Re_0}{\Re}\right)^{3\gamma}\frac{\mathbf{f}_p(\xi,\theta,\varphi)}{\Re},$$

$$\mathbf{F}_g = -\rho_0\left(\frac{\Re_0}{\Re}\right)^3\widetilde{\rho}(\xi,\theta,\varphi)\frac{GM_g}{\Re^2\xi^2}\mathbf{e_r},$$

where $\mathbf{f}_B$ and $\mathbf{f}_p$ are vector functions not depending explicitly on time, and $B_0^2 = B_{r0}^2 + B_{\theta 0}^2 + B_{\varphi 0}^2$. With $\gamma = 4/3$, all the terms in the right part of (A5) change synchronously with time. Just this circumstance determines the existence of the self-similar solution when three independent forces $\mathbf{F}_B$, $\mathbf{F}_p$, and $\mathbf{F}_g$ act simultaneously. Then we put $\gamma = 4/3$ and represent equation (A5) in the following form:

$$\frac{d^2\Re}{dt^2}\mathbf{e_r} = \frac{1}{\Re^2}\left\{\frac{B_0^2}{4\pi\rho_0}\frac{\Re_0\mathbf{f}_B}{\widetilde{\rho}\xi} - \frac{p_0}{\rho_0}\frac{\Re_0\mathbf{f}_p}{\widetilde{\rho}\xi} - \frac{GM_g}{\xi^3}\mathbf{e_r}\right\}. \tag{A6}$$

Since the expression inside the curled brackets does not depend on time explicitly and $d/dt = (d/d\Re)(d\Re/dt)$, instead of (A6) we obtain

$$\Re^2 U\frac{dU}{d\Re} = \alpha = const, \quad U = \frac{d\Re}{dt}. \tag{A7}$$

The solution of (A7) is an expression

$$U^2 = U_0^2 + \frac{2\alpha}{\Re_0}\left(1 - \frac{\Re_0}{\Re}\right), \tag{A8}$$

where U_0 is the initial velocity of the leading edge of the expanding volume, $U_0 = U(\Re = \Re_0)$. The sense of α is determined by the sense of the sum of forces in the right part of (A5). With the CME size infinitely increasing with time, $\Re \to \infty$, $2\alpha/\Re_0 = U_\infty^2 - U_0^2$, and (A8) takes the form

$$U^2 = U_0^2\left(\frac{\Re_0}{\Re}\right) + U_\infty^2\left(1 - \frac{\Re_0}{\Re}\right), U_\infty = U(\Re \to \infty). \tag{A9}$$

The ultimate velocity U_∞ can be estimated from experiment by comparing it with the CME speed at $\Re \gg \Re_0$. For a CME to which a gradual acceleration of a filament visible in Hα corresponds, one should put $U_0 = 0$ in (A9). Then the $\Re$ and t are related with each other by an expression

$$\frac{t - t_0}{\tau} = \sqrt{x}\sqrt{x-1} + \ln\left(\sqrt{x} + \sqrt{x-1}\right), \tag{A10}$$

where

$$\tau = \frac{\Re_0}{U_\infty}, \quad x = \frac{\Re}{\Re_0}.$$

If $\Re$ does not exceed some value, $\Re_{max} > \Re_0$, or $U(\Re = \Re_{max}) = 0$, then

$$\frac{2\alpha}{\Re_0} = -U_0^2\left(1 - \frac{\Re_0}{\Re_{max}}\right)^{-1}$$

in (A8). Expression (A8) also contains a solution corresponding to the compression up to the size $\Re_{min} < \Re_0$.

[41] To demonstrate the self-similar expansion of the structural components of a CME, which is not obvious from implicit expressions (A8) and (A9), we show in Figure 6 invariant kinematic plots: radial distance R, velocity U, and acceleration a versus time. These plots are independent of the initial size R_0, the asymptotic velocity U_∞, and the start time of the motion t_0. The left column shows the extended initial part, and the right column shows a wider range of times and heights. These curves have been calculated numerically.

[42] Expression (A8) can be obtained from the conservation of the total energy E_0 contained in the expanding plasma of mass $m = const$. From (A1), (A2), and (A3) we obtain

$$E_0 = \frac{m\langle v^2\rangle}{2} + m\left\langle\frac{p}{\rho(\gamma-1)}\right\rangle + m\left\langle\frac{B^2}{8\pi\rho}\right\rangle - \cdot GM_g\int\frac{dm}{r} = \frac{m\langle v^2\rangle}{2} + m\left\langle\frac{p}{\rho(\gamma-1)}\right\rangle_0\left(\frac{\Re_0}{\Re}\right)^{3\gamma-3} + \cdot m\left\langle\frac{B^2}{8\pi\rho}\right\rangle_0\left(\frac{\Re_0}{\Re}\right) - \frac{GM_g m}{\Re}\widetilde{g}. \quad \text{(A11)}$$

Here, the angle brackets denote the averaging of the corresponding quantities over the whole mass m. The number $\widetilde{g}$ is determined by the initial mass distribution over the CME volume, $\widetilde{g} = (\Re/m)\int dm/r$. By putting $\gamma = 4/3$, $v(\Re = \Re_0) = v_0$, and excluding $2E_0/m$ from (A11), we find

$$\langle v^2\rangle = \langle v_0^2\rangle + \left(\frac{2}{\gamma(\gamma-1)}C_0^2 + V_{a0}^2 - \frac{2GM_g}{\Re_0}\widetilde{g}\right)\left(1 - \frac{\Re_0}{\Re}\right), \quad \text{(A12)}$$

with $C_0 = \sqrt{\left\langle\frac{\gamma p}{\rho}\right\rangle_0}$ and $V_{a0} = \sqrt{\left\langle\frac{B^2}{4\pi\rho}\right\rangle_0}$ being the average initial sound and Alfvén speeds.

[43] From the comparison of (A8) and (A12), the meaning of α becomes clear. One should keep in mind herewith that due to (A4), the average mass velocity $\sqrt{\langle v^2\rangle}$ remains always less than the velocity U of the leading edge of the expanding volume. Their relation depends of the spatial distribution of the density, temperature, and the magnetic field at the onset of the expansion.

[44] The expressions corresponding to the self-similar solution do not describe the initial stage of the expansion for a real CME from the solar surface. Moreover, gravity at this stage is not a central force, and it is determined by the mass of the Sun $M_\odot$. Nevertheless, the use of $2GM_\odot/R_\odot$ instead of $(2GM_g/\Re_0)\widetilde{g}$ in (A12) probably results in a correct conclusion about the existence of a solution to describe the expansion of a CME from the solar surface up to, e.g., Earth orbit. With such a replacement in (A12) and a condition $v_0 \approx 0$ typical for CMEs, we find

$$\langle v_\infty^2\rangle = \langle v^2\rangle_{\Re\to\infty} \approx \left(\frac{2}{\gamma(\gamma-1)}C_0^2 + V_{a0}^2 - \frac{2GM_\odot}{R_\odot}\right). \quad \text{(A13)}$$

Now C_0^2 and V_{a0}^2 should be interpreted as their average values inside some large volume of a characteristic size $\Re_0$ inside which a CME was generated. The quantity $2GM_\odot/R_\odot$ is equal to $2V_1^2 = V_{esc}^2$, where $V_{esc} \approx 618$ km/s is the escape velocity at the solar surface. If the term in large parentheses in (A13) is positive, then unlimited expansion of the CME is possible. With $\gamma = 4/3$ this condition becomes $(4.5C_0^2 + V_{a0}^2 - V_{esc}^2) > 0$. With the coronal temperature of 2 MK, the value $C_0 = 210$ km/s, and the above condition is satisfied with $V_{a0} > 291$ km/s.

[45] **Acknowledgments.** This research was supported by the Russian Foundation for Basic Research (grant 03-02-16591) and the Russian Ministry of Science and Technical Policy (grant 477.2003.2), and the Federal Scientific Program "Astronomy," and by NASA under NAS 5-98033. We are grateful to the instrumental teams operating SOHO/EIT-LASCO, the Siberian Solar Radio Telescope, and the Big Bear Solar Observatory for data used here. The CME catalog used in this study is generated and maintained by the Center for Solar Physics and Space Weather, The Catholic University of America in cooperation with the Naval Research Laboratory and NASA. SOHO is a project of international cooperation between ESA and NASA. *Yohkoh* is a project of international cooperation between ISAS, NASA, and SERC (now PPARC).

[46] Shadia Rifai Habbal thanks Simon P. Plunkett and Volker Bothmer for their assistance in evaluating this paper.

References

Barenblatt, G. I. (1978), *Similarity, Self-Similarity, and Intermediate Asymptotics* (in Russian), 207 pp., Gidrometeoizdat, Leningrad.

Chertok, I. M., V. V. Grechnev, H. S. Hudson, and N. V. Nitta (2004), Homologous large-scale activity in solar eruptive events of 24–26 November 2000, *J. Geophys. Res.*, *109*, A02112, doi:10.1029/2003JA010182.

Cremades, H., and V. Bothmer (2004), On the three-dimensional configuration of coronal mass ejections, *Astron. Astrophys.*, *422*, 307.

Dere, K. P., et al. (1997), EIT and LASCO Observations of the Initiation of a Coronal Mass Ejection, *Solar Phys.*, *175*(2), 601–612.

Gallagher, P. T., G. R. Lawrence, and B. R. Dennis (2003), Rapid acceleration of a coronal mass ejection in the low corona and implications for propagation, *Astrophys. J.*, *588*(1), L53–L56.

Grechnev, V. V., et al. (2003), The Siberian Solar Radio Telescope: the current state of the instrument, observations, and data, *Solar Phys.*, *216*(1), 239–272.

Harrison, R. A., P. Bryans, G. M. Simnett, and M. Lyons (2003), Coronal dimming and the coronal mass ejection onset, *Astron. Astrophys.*, *400*, 1071–1083.

Hudson, H. S., L. W. Acton, K. L. Harvey, and D. E. McKenzie (1999), A stable filament cavity with a hot core, *Astrophys. J.*, *513*, L83–L86.

Kano, R. (1994), The time evolution of X-ray structure during filament eruption, in *X-ray Solar Physics from Yohkoh*, edited by Y. Uchida et al., p. 273, Universal Acad. Press, Tokyo.

Khan, J. I., and H. S. Hudson (2000), Homologous sudden disappearances of transequatorial interconnecting loops in the solar corona, *Geophys. Res. Lett*, *27*, 1083.

Low, B. C. (1982), Self-similar magnetohydrodynamics. I – The gamma = 4/3 polytrope and the coronal transient, *Astrophys. J.*, *254*, 796–805.

Martin, S. F. (1998), Conditions for the formation and maintenance of filaments (invited review), *Solar Phys.*, *182*, 107–137.

Neupert, W. M. (2002), Acceleration of coronal mass ejections in the low corona and association with surface activity, 200th AAS Meeting, *Bull. Am. Astron. Soc.*, *34*, 693.

Sedov, L. I. (1981), *Similarity Methods and Dimensional Analysis in Mechanics* (in Russian), 9th ed., 448 pp., Nauka, Moscow.

Smolkov, G. I., A. A. Pistolkors, T. A. Treskov, B. B. Krissinel, and V. A. Putilov (1986), The Siberian solar radio-telescope—Parameters and principle of operation, objectives and results of first observations of spatio-temporal properties of development of active regions and flares, *Astrophys. Space Sci.*, *119*(1), 1–4.

Uralov, A. M., S. V. Lesovoi, V. G. Zandanov, and V. V. Grechnev (2002), Dual-filament initiation of a Coronal Mass Ejection: Observations and model, *Solar Phys.*, *208*(1), 69–90.

Wang, H., Y. Yan, T. Sakurai, and M. Zhang (2000), Topology of magnetic field and coronal heating in solar active regions – II. The role of quasi-separatrix layers, *Solar Phys.*, *197*(2), 263–273.

Zel'dovich, Y. B., and Y. P. Raizer (1966), *Physics of Shock Waves and High-Temperature Hydrodynamic Phenomena* (in Russian), 2nd ed., 686 pp., Nauka, Moscow.

V. V. Grechnev and A. M. Uralov, Institute of Solar-Terrestrial Physics, SB, RAS, P.O. Box 4026, Irkutsk 664033, Russia. (uralov@iszf.irk.ru; grechnev@iszf.irk.ru)

H. S. Hudson, Space Sciences Laboratory, University of California, Berkeley, CA 94720, USA. (hhudson@ssl.berkeley.edu)